Journal of Catalysis 375 (2019) 448–455

Contents lists available at ScienceDirect

Journal of Catalysis

journal homepage: www.elsevier.com/locate/jcat

Origin and prevention of broad particle size distributions in carbon-supported palladium catalysts prepared by liquid-phase reduction

Wouter S. Lamme [a], Onno van der Heijden [a], Nynke A. Krans [a], Erica Nöllen [b], Nathalie Mager [c], Sophie Hermans [c], Jovana Zečević [a], Krijn P. de Jong [a,*]

[a] Inorganic Chemistry and Catalysis, Debye Institute for Nanomaterials Science, Utrecht University, Universiteitsweg 99, 3584 CG Utrecht, the Netherlands
[b] Catalysis Research GCC/PB, BASF Nederland B.V., Strijkviertel 61, 3454 ZG De Meern, the Netherlands
[c] IMCN Institute, Université catholique de Louvain, Place L. Pasteur 1, 1348 Louvain-la-Neuve, Belgium

ARTICLE INFO

Article history:
Received 27 April 2019
Revised 15 June 2019
Accepted 17 June 2019
Available online 3 July 2019

Keywords:
Palladium
Carbon
Surface functionalization
Adsorption
Heterogeneous catalysis
Supported catalysts
Catalyst preparation
Hydrogenation

ABSTRACT

Carbon-supported palladium (Pd/C) catalysts often display broad or multimodal Pd particle size distributions detrimental for their performance. Therefore, the formation of large particles during preparation should be better understood and avoided. We prepared catalysts with up to 10 wt% Pd supported on oxygen-functionalized carbon nanotubes and activated carbon via liquid-phase reduction. It was inferred that small Pd particles (~1 nm) were formed from Pd ions adsorbed on the carbon. At higher loadings, up to 65% of the Pd ended up in larger particles (>10 nm) probably formed from Pd ions in solution, lowering the Pd-normalized activity in the hydrogenation of cinnamaldehyde 4-fold compared to samples with small particles only. Three key factors were identified for preparing Pd/C catalysts with exclusively ~1 nm Pd particles: a support with a high density of acid sites and high specific surface area, and a metal loading at molar ratio Pd/acid sites <0.5.

1. Introduction

Metal catalysts supported on a solid support material (e.g. Al_2O_3, SiO_2, C) are of great importance in industry [1–3]. Carbon-supported palladium (Pd/C) catalysts are widely used for hydrogenation reactions for the production of fine chemicals [4,5]. Like with all supported metal catalysts, the performance of a Pd/C catalyst is strongly determined by the catalyst structure. For high activity, a high metal surface area is often desired which is accomplished by reducing the size of metal particles to nanometer scale and increasing the metal loading. To prevent particle growth via migration and coalescence and/or Ostwald ripening, the metal nanoparticles should be uniformly distributed over the support and have narrow particle size distributions [6,7]. However, broad or multimodal particle size distributions are frequently observed with carbon-supported Pd catalysts [8–16].

Catalyst preparation methods play a key role in achieving the desired structural properties of supported catalysts [17]. For carbon-supported metal catalysts, it has long been known that the surface chemistry of the support strongly influences the preparation of the supported metal catalyst [18]. Due to the high cost of precious metals, high metal dispersions are especially important for precious metal catalysts such as Pd/C. Higher dispersions can be obtained by adding functional groups to the support surface, which can act as adsorption sites for the metal precursor [8,13,19–21]. However, to the best of our knowledge, no systematic study has been performed where a correlation between the number of functional groups on the support surface, the metal loading and the catalyst structure has been established.

Preparation of Pd/C catalysts often comprises two steps: the metal precursor is first loaded onto a support and then reduced [22]. It has been previously found that the reduction method is more critical than the metal loading method [23]. Reduction in the gas phase with H_2 at elevated temperatures typically leads to uniformly distributed metal particles with a narrow size distribution [22–24]. However, upscaling the gas phase reduction of carbon-supported catalysts is challenging and therefore performing reduction in liquid phase is highly desirable for industrial applications. Reduction in the liquid phase, however, often causes non-uniform distributions of the metal particles across the support and broad particle size distributions, both for Pd/C [10,11,23] and for Pt/C [25]. Specifically, preparation of carbon nanotubes-supported Pd catalysts (Pd/CNT) by reduction with sodium borohy-

* Corresponding author.
E-mail address: k.p.dejong@uu.nl (K.P. de Jong).

https://doi.org/10.1016/j.jcat.2019.06.034
0021-9517/

dride yielded bimodal particle size distributions with particles of ~1 nm and >10 nm in size [23]. The formation of the particles larger than 10 nm was not fully understood. Similar results have been obtained for Pt/C prepared by liquid-phase reduction by sodium borohydride [25], where the formation of small particles was explained by adsorption of the metal precursor and the formation of large particles by reduction from the liquid phase by the addition of a reducing agent. It was hypothesized that a similar process occurred during the preparation of Pd/CNT catalysts: at low Pd loadings complete adsorption of the precursor occurs, and subsequent reduction by sodium borohydride leads to a unimodal particle size distribution. At higher Pd loadings, reduction of precursor species in solution might take place, followed by precipitation of large particles on the support.

To systematically investigate the effects of liquid phase reduction on the particle size distribution, we prepared carbon nanotubes (CNT) and activated carbon (AC) supported Pd catalysts with a range of Pd loadings. For most samples, the carbon support materials were first functionalized by liquid-phase oxidation (LPO) to create oxygen-containing functional groups on the surface and investigate their impact on Pd nanoparticle dispersion. Pd was loaded on C by a one-pot two-step approach: first, the precursor, $(NH_3)_4Pd(NO_3)_2$, was added to an aqueous carbon suspension at pH 11, allowing ion adsorption on deprotonated acidic functional groups on the support surface. This was followed by liquid-phase reduction using either formaldehyde or sodium borohydride as reducing agent. It was shown that the metal loading, and thus molar ratios between metal precursor and acidic support functional groups (M/A), play a key role in metal dispersion. At an M/A ratio of 0.5, corresponding to 2 functional acid groups per Pd^{2+} ion, maximum ion adsorption is achieved, and well dispersed particles were formed upon subsequent reduction. Higher Pd loadings were seen to lead to formation of larger Pd particles, likely caused by reduction of Pd ions directly in the solution and subsequent deposition onto a support. The nature of the reducing agent also influenced the metal dispersion.

2. Materials and methods

2.1. Materials and reagents

The multi-walled carbon nanotubes (CNT) used were Baytubes C 150 HP obtained from Bayer Materials Science. The activated carbon (AC) was an HCl-washed High Purity carbon from BASF. Nitric acid (65 wt%), HCl (fuming), aqueous NH_3 (28–30 wt%) and NaOH were purchased from Merck (Emsure, p.a.); urea (p.a.), KCl (p.a.) and *trans*-cinnamaldehyde (99%) from Acros; 2-propanol (puriss., ≥99.5%), sodium borohydride (≥98%) and aqueous formaldehyde (37 wt%, stabilized with methanol) from Sigma Aldrich. Biphenyl (99%) and an aqueous $(NH_3)_4Pd(NO_3)_2$ solution containing 4.6 wt % Pd (50 g L^{-1}) were acquired from Alfa Aesar.

2.2. Carbon support pre-treatment

Surface functionalization of the carbon materials was performed by liquid-phase oxidation (LPO). This functionalization treatment was performed by refluxing 4 g carbon in 150 mL boiling 65 wt% nitric acid for 1.5 h (CNT) or 30 wt% nitric acid for 0.5 h (AC). Afterwards, the functionalized carbons were isolated from the reaction mixture by filtration and washed thoroughly with demineralized water. Functionalized carbon supports were dried in an oven at 120 °C in static air for at least 16 h prior to use.

2.3. Metal deposition

The procedures for Pd/C catalyst preparation were based on literature [8,23]. 0.4 g functionalized or nonfunctionalized carbon was suspended in 90 mL demineralized water in a round-bottom flask, and magnetically stirred. The pH was adjusted to 11 using 28–30 wt% NH_3 (aq) aiming at a net negatively charged carbon surface, and the suspension was stirred for at least 2 h. To prepare catalysts with different Pd loadings (1–15 wt%), different volumes of aqueous $(NH_3)_4Pd(NO_3)_2$ were added, and the mixtures were stirred for another 24 h. Subsequently, excess amounts of aqueous reducing agent solutions were added at room temperature. Formaldehyde (37 wt%, 0.8–3 mL) was added instantly. Freshly prepared aqueous sodium borohydride (2.3–8 mg $NaBH_4$) was added through a flexible tube below the reaction mixture surface at a rate of 0.4 mg sodium borohydride/min using a syringe pump. After adding formaldehyde, the reaction mixture was heated to 80 °C for 1 h. In case of addition of sodium borohydride, the reaction mixture was stirred at room temperature for 1 h.

The samples were 5 times washed and filtered using demineralized water and a Büchner funnel and then dried at 120 °C in static air for 16 h.

Samples were labeled xPd/S_R in which x is the Pd loading (wt. %, from ICP-OES), S is the support (CNT for pristine CNT, CNT-Ox for LPO-functionalized CNT, AC for as-received and HCl washed AC or AC-Ox for LPO-treated activated carbon), and R is the reducing agent (H = sodium borohydride or F = formaldehyde).

2.4. Characterization

2.4.1. N_2 Physisorption

Nitrogen physisorption measurements were performed on a Micromeritics Tristar 3000 instrument at −196 °C. Before the measurements, samples were dried for 14 h at 120 °C under flowing N_2. Support surface areas were calculated using the multipoint BET method ($0.05 < p/p_0 < 0.25$). Pore volumes were determined at $p/p_0 = 0.997$ and pore sizes were determined by the Barrett–Joyner–Halenda (BJH) method by using the adsorption branches of the isotherms.

2.4.2. Potentiometric titration

The amount of acidic functional groups on the support surface was determined by performing potentiometric titrations [26]. 30 mL 0.1 M KCl (aq) was added to 25 mg crushed sample to increase the conductivity of the suspension. The suspension was ultrasonically dispersed for 30 min. Titration was performed using a Radiometer Analytical TIM880 setup, continuously stirring and flushing with N_2. Additional 35 mL of 0.1 M KCl (aq) was added prior to titration to ensure that the pH electrode was fully immersed. The sample was titrated using a 0.01 M NaOH/0.1 M KCl solution as titrant until the pH of the mixture reached 9. The amount of titrant at the inflection point (equal to the amount of acidic groups) was determined by numerically calculating the first derivative of the titration curve and then applying a second degree polynomial fit ($dpH/dV = aV^2 + bV + c$) around the maximum (typically around pH 7), finding the volume of titrant at the inflection point by calculating $V_{inflection} = -b/2a$.

2.4.3. XPS

X-ray photoelectron spectroscopy (XPS) was carried out on an SSX 100/206 photoelectron spectrometer from Surface Science Instruments (USA) equipped with a monochromatized microfocused Al X-ray source (powered at 20 mA and 10 kV). The powder samples were fixed on small brass cups using double-sided adhesive tape and then placed on an insulating homemade ceramic

sample holder (Macor, Switzerland). A flood gun set at 8 eV and a Ni grid placed 3 mm above the sample surface were used for charge stabilisation. The analyzed area was approximately 1.4 mm^2, and the pass energy was set at 150 eV. The binding energies were set by fixing the C_{1s} peak [C-(C,H) component] at 284.8 eV. Four photopeaks (C_{1s}, O_{1s}, N_{1s}, $Pd_{3d5/2}$) were analyzed. Data treatment was performed using the CasaXPS program (Casa Software Ltd), and a sum of Gaussian/Lorentzian (85/15) components after subtraction of a Shirley-type baseline. Molar fractions were calculated using peak areas normalised based on acquisition parameters and sensitivity factors provided by the manufacturer.

2.4.4. TEM

(Scanning) transmission electron microscopy ((S)TEM) imaging was performed on an FEI Talos F200X transmission electron microscope, operated at 200 kV and equipped with a high-brightness field emission gun (X-FEG). Pd particle size distributions were determined by measuring typically 100–200 nanoparticles using ImageJ from which the number-average particle size was calculated.

2.4.5. XRD

X-ray diffraction (XRD) was performed on a Bruker D2 PHASER using Co Kα radiation (λ = 1.789 Å). Diffractograms were measured from 10° to 90° 2θ in 0.1° increments. Pd crystallite sizes were calculated in Bruker Topas software using the (1 1 1) diffraction line at 46.9° 2θ. Due to overlap between the Pd (1 1 1) and C (1 0 0) peaks, the XRD patterns were deconvoluted using the Double-Voigt approach comprising of Lorentzian and Gaussian component contributions. Reported sizes are volume weighted mean sizes based on the integral breadth [23,27]. The amount of Pd in larger crystallites was estimated by normalizing the area of the Pd (1 1 1) diffraction peak against C (1 0 0) and (1 0 1) after deconvolution of the XRD pattern in Bruker Topas software. This is described in more detail in the supporting information.

2.4.6. H_2 chemisorption

H_2 chemisorption measurements were performed on a Micromeritics ASAP 2020C instrument. Samples were reduced at 90 °C in flowing H_2 for 1 h and subsequently evacuated at 150 °C. The H_2 uptake was measured at 90 °C. To account for hydride formation at higher pressure (300 mbar and up), extrapolations to zero pressure were performed on logarithmic fits that were applied to the data points up to 150 mbar. For the calculations (hemi) spherical particles, an H:Pd stoichiometry of 1 and an atomic cross section of Pd of 0.0787 nm^2 were used.

2.4.7. ICP-OES

Inductively coupled plasma-optical emission spectroscopy (ICP-OES) measurements were performed with a SPECTRO ARCOS ICP-OES instrument after dissolving the samples in aqua regia.

2.5. Catalytic tests

Samples were tested for the hydrogenation of cinnamaldehyde in an Autoclave Engineers EZE-Seal batch reactor system fitted with a separate vessel that was used for preheating and pressurizing the reagent. The separate vessel allowed a well-defined reaction starting time by injecting the reagent to a heated and pressurized reactor. The catalyst (30 mg) and 47 g 2-propanol were loaded in the reactor; 1.6 g *trans*-cinnamaldehyde, a solution of 60 mg biphenyl (as internal standard) and 1.5 g demineralized water in 22 g 2-propanol was loaded in the separate vessel. Reactor and vessel were heated to 60 °C while flushing with N_2 and were then pressurized with H_2 to 15 bar (reactor) and 25 bar (vessel). Then the contents of the vessel were released into the reactor. The reactor was kept at 60 °C and 20 bar H_2 pressure (flowing at 100 mL_n min^{-1}) for 3–4 h. 0.5 mL liquid samples were taken from the reaction mixture at selected intervals and analyzed by gas chromatography (Shimadzu GC-2010 fitted with an Agilent CP–Wax 57 CB column). More details on selectivity and activity calculations are described in the supporting information.

3. Results and discussion

3.1. Support characteristics

Properties of the support materials used in this study were assessed using N_2 physisorption and titration (Table 1). After functionalization by LPO the BET surface area of the CNT increased, which was likely caused by etching of the surface with acid, causing it to roughen. For the activated carbon, the surface area and pore volume both decreased after LPO, which could have been caused by oxidation and collapse of pillar-like structures that ensure structural integrity of pristine activated carbon. As expected, the LPO treatment led to a significant increase in number and density of acidic functional groups on both CNT and AC supports.

The surface functional groups nature was further investigated using XPS for CNT and CNT-Ox. The untreated CNT contained a low amount of oxygen (1.4 at.%). This increased to 6.3 at.% for CNT-Ox. Deconvolution of the C_{1s} peak showed an increase in phenolic, carbonyl and carboxyl functional groups. This is described in more detail in the supporting information.

3.2. Structure of the catalysts

To investigate the effects of reducing agents, support functionalization and Pd loading on the Pd particle size distribution, in particular on the formation of large Pd particles, a set of catalysts was prepared with nominal Pd loadings varying from 1 to 19 wt%. As described in the Experimental section, the carbon supports were functionalized, and the pH was set at 11 to facilitate the adsorption of Pd precursor cations. As reducing agents, sodium borohydride and formaldehyde were used. All samples were dried at 120 °C in static air unless specified differently. Properties of the prepared catalysts are summarized in Table 2.

3.2.1. Structure of CNT-supported catalysts

The first five samples listed in Table 2 were prepared using CNT-Ox as support and formaldehyde as reducing agent. As can be seen from ICP results, at low nominal loading (≤2 wt%) all Pd was

Table 1
Textural and acidic properties of support materials.

Support	BET surface area (m^2 g^{-1})	Pore volume (cm^3 g^{-1})	Acidic functional groups (mmol g^{-1})	Acidic functional groups density (nm^{-2})
CNT	200	1.2	0.02	0.007
CNT-Ox	270	1.2	0.70	1.6
AC	860	1.9	0.01	0.06
AC-Ox	704	1.1	1.2	1.0

Table 2
Pd/C catalyst properties.

Sample	Pd loading			Particle/crystallite size (nm)		
	Nominal (wt%)	ICP (wt%)	M/A[a]	XRD	TEM (sub-10 nm)	H_2 chemisorption
1Pd/CNT-Ox_F	1.3	1.3	0.17	–	0.9 ± 0.2	0.7
2Pd/CNT-Ox_F	2.0	1.8	0.24	–	1.4 ± 0.3	0.8
4Pd/CNT-Ox_F	5.5	3.9	0.54	–	0.8 ± 0.3	0.6
4Pd/CNT-Ox_F-2	11.2	3.7	0.48	–	1.4 ± 0.3	0.8
4Pd/CNT-Ox_F-3	15.4	3.9	0.54	–	1.0 ± 0.2	0.8
1Pd/CNT-Ox_H	2.1	1.0	0.14	–	1.5 ± 0.4	1.4
2Pd/CNT-Ox_H	3.5	2.4	0.33	–	0.8 ± 0.2	1.0
4Pd/CNT-Ox_H	5.7	4.4	0.61	2.9	1.1 ± 0.3	2.0
8Pd/CNT-Ox_H	11.0	7.9	1.15	5.2	0.6 ± 0.2	1.8
10Pd/CNT-Ox_H	15.4	9.6	1.43	4.8	1.0 ± 0.3	2.9
4Pd/AC-Ox_H	4.8	4.3	0.35	–	0.7 ± 0.2	0.3
7Pd/AC-Ox_H	11.8	7.4	0.63	–	0.8 ± 0.2	0.8
10Pd/AC-Ox_H	19.1	10.3	0.90	9.5	0.9 ± 0.2	0.9
5Pd/CNT_H	5.5	4.6	23	2.9	~6[b]	n.d.
1Pd/CNT_F	5.5	1.4	7	4.0	~3[b]	n.d.

[a] Defined as the molar ratio between Pd (determined by ICP) and acidic functional groups on the unloaded support (determined by titration).
[b] Very heterogeneous sample (see Fig. 2).

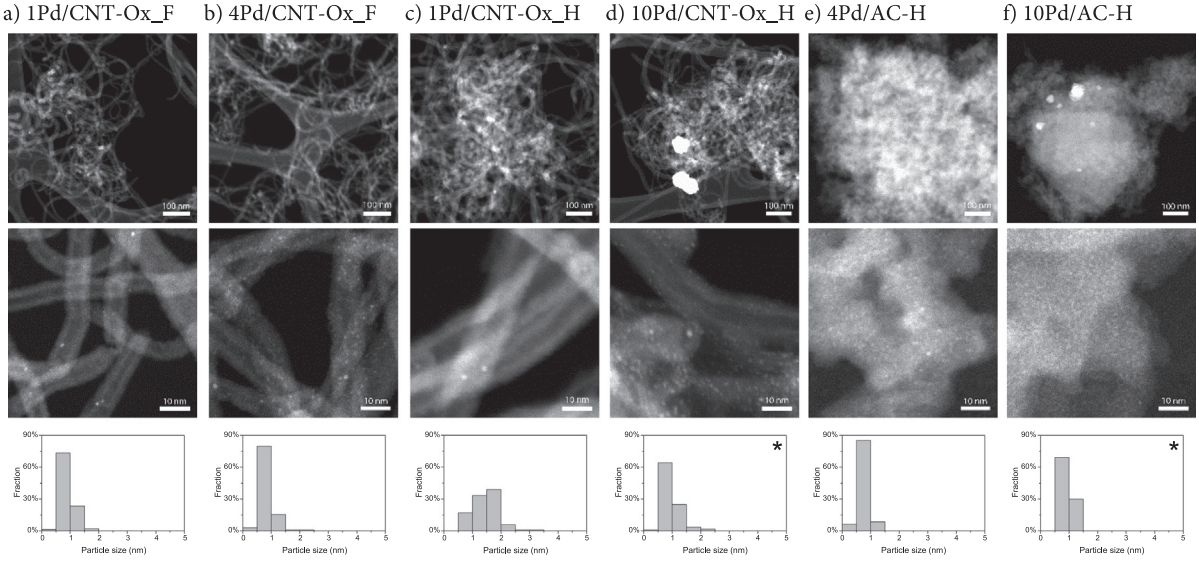

Fig. 1. Representative high-angle annular dark-field scanning transmission electron microscopy (HAADF-STEM) images and particle size distribution histograms of Pd/C catalysts. (*) Only sub-10 nm particles were included in the particle size distribution of the 10 wt% sodium borohydride-reduced samples.

deposited whereas at higher nominal Pd loading (up to 15 wt%), catalysts that were reduced by formaldehyde had a maximal Pd loading of 3.9 wt%. XPS measurements revealed that the samples contained both Pd^0 and Pd^{II} (Table S3, Figs. S3–S6), proving that metallic Pd was present and thus that reduction had taken place; the Pd^{II} was likely formed by surface oxidation due to air exposure after reduction. Average Pd particle sizes determined by H_2 chemisorption were similar for all the xPd/CNT-Ox_F catalysts, with 0.8 nm on average. A slightly larger average Pd particle size of about 1 nm was determined by scanning transmission electron microscopy (STEM) (Fig. 1a and b, Fig. S7a). This discrepancy can be ascribed to the fact that particles of less than 0.5 nm were not detected in STEM or to an increased H:Pd stoichiometry (>1) leading to a decrease in average Pd size determined by H_2 chemisorption. Importantly, STEM images showed that Pd particles were uniformly distributed across the CNT-Ox support and that no agglomeration was observed even at the highest achieved Pd loading (3.9 wt%). Due to the sub-nanometer size, Pd particles in xPd/CNT-Ox_F samples could not be detected by XRD (Table 2, Fig. S9c). When nonfunctionalized CNTs were used as support, the extent of deposition of the metal precursor was much lower than when functionalized CNTs were used (sample 1Pd/CNT_F, Table 2). Even though nominal loading was set to 5.5 wt%, ICP detected only 1.4 wt% of Pd. Some Pd particles with a size around 1 nm were observed as well as a significant number of larger particles (>5 nm, Fig. 2a), the latter being confirmed by XRD (Fig. S9e). We ascribe this to the absence of functional groups leading to less Pd ion adsorption and weaker interaction with the support which likely caused Pd particles to grow to larger size. On the other hand, the presence of functional groups seems to promote and strengthen the attachment of Pd ions preventing the formation of large Pd particles.

Like samples reduced by formaldehyde, reduction by sodium borohydride also led to Pd loadings on CNT-Ox samples to be lower than nominally set. However, higher maximal Pd loadings were achieved, namely 7.9 wt% and 9.6 wt% when nominal loadings were set to 11 wt% and 15 wt%, respectively (Table 2). Large differences compared to formaldehyde-reduced samples can be seen from STEM images (Fig. 1c and d, Figs. S7b–d): next to uniformly distributed particles of ~1 nm visible for all samples, STEM images of the sodium borohydride-reduced samples with higher loadings also revealed particles larger than 10 nm. High magnification STEM

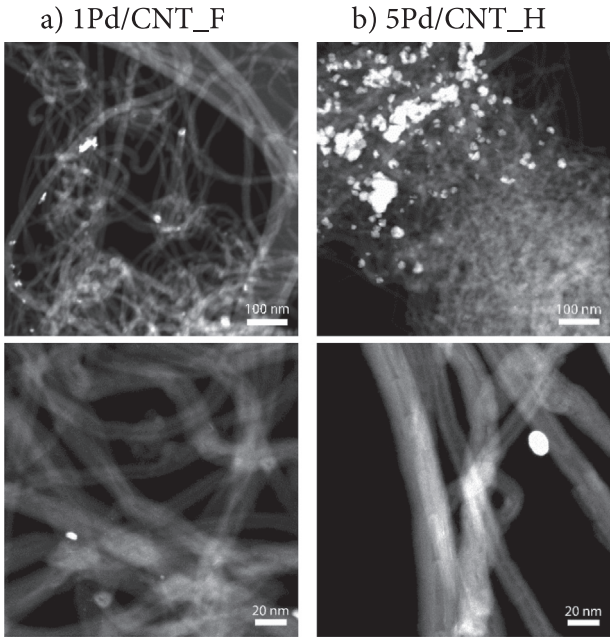

Fig. 2. Representative high-angle annular dark-field scanning transmission electron microscopy (HAADF-STEM) images of Pd/CNT catalysts prepared using nonfunctionalized CNT as support. Reduction of the metal precursor was performed in liquid phase by (a) formaldehyde, (b) sodium borohydride.

and TEM images showed that the large particles were polycrystalline (Fig. S11), indicating that these particles could have been formed by agglomeration of smaller particles rather than growing as a single crystal. The average particle sizes determined by H_2 chemisorption increased with increasing loading (Table 2). XPS measurements revealed that the samples contained both Pd^0 and Pd^{II} (Table S3, Figs. S3–S6), proving that metallic Pd was present and thus that reduction had taken place; the Pd^{II} was likely formed by surface oxidation due to air exposure after reduction. The concentration of metallic Pd increased with increasing loading, which could be ascribed to the increased average particle size at higher loading: due to the larger particles, a smaller fraction of Pd atoms is subject to air exposure and consequently a larger fraction stays metallic. X-ray diffraction peaks for Pd were observed for samples with higher Pd loadings (Fig. S9a, c and d). While ~1 nm Pd particles were not detected in XRD, the presence of large Pd particles could be assessed from the XRD patterns. However, due to the polycrystalline nature of the larger particles, the crystallite size, as determined from XRD, is much smaller than those from STEM image analysis (Table 2). From the presence of sharp Pd diffraction lines in the XRD patterns it can be concluded that the larger particles were metallic Pd. When nonfunctionalized CNT was used as a support, only large Pd particles were observed (>10 nm, Fig. 2b), confirming the hypothesis based on formaldehyde reduced samples, that the functional groups impact the attachment of metal ions and the consequent size of the metal particles.

The formation of 1 nm particles was studied by in situ heating electron microscopy. Very few particles were observed in a 4Pd/CNT-Ox_H sample that was dried at room temperature. Upon heating, particles appeared and grew (Fig. S8). This implies the presence of sub-nm particles and probably atomically dispersed Pd species after reduction. It is concluded that the 1 nm particles are formed during the 120 °C drying treatment. As the XPS measurements showed that metallic Pd was present in the samples, we believe the 1 nm particles are formed by agglomeration of subnanometric particles (Pd clusters) and atomically dispersed species. Upon heating, any non-metallic Pd can be reduced by either traces of reducing agent and/or the carbon support to become mobile and then captured by Pd clusters to form the ~1 nm particles.

3.2.2. Structure of AC-supported catalysts

Next to CNTs, functionalized activated carbon (AC-Ox) was also used as a support for sodium borohydride-reduced catalysts. Pd loadings were again lower than nominal, e.g. for the sample with the nominal loading of 19 wt%, the measured loading was 10 wt %. STEM images show particle sizes and particle distributions like those of the sodium borohydride-reduced CNT-Ox-supported catalysts: next to uniformly distributed particles of ~1 nm visible for all samples (Fig. 1e and f, Fig. S7e), large particles (>10 nm) were observed in the sample with the highest loading (Fig. 1f). Furthermore, like the xPd/CNT-Ox_H samples, Pd diffraction peaks in the XRD patterns were only observed at higher loading (Fig. S9d). However, the Pd loading at which larger particles started forming was higher on AC-Ox: both the 4 wt% and 7 wt% Pd sample showed no evidence of the formation of large particles, whereas the 10 wt% Pd sample did.

From the results above, it is clear that both the functionalization of the CNT support and the nature of the reducing agent play an important role in determining the achievable Pd loading and Pd particle size distribution.

3.3. Impact of support functionalization

First, we consider the impact of support functionalization. The conditions during catalyst preparation were such that the acidic functional groups on the support surface were deprotonated and negatively charged allowing ion adsorption or electrostatic interaction of Pd ions. As the Pd ion has a 2+ charge and deprotonated carboxylic and phenolic functional groups have a 1− charge, 1 Pd ion could bind to 2 acidic functional groups. This implies that at Pd ions to acid functional groups molar ratios (M/A) of 0.5 and below, all Pd ions should be adsorbed to the support surface. For CNT-Ox, the Pd loading corresponding to this threshold ratio is 4 wt%, which was also the maximum achieved loading in samples reduced by formaldehyde. It was argued that upon reduction, the adsorbed Pd ions are expected to form uniformly distributed small Pd particles since their interaction with the support is strong. This was indeed observed for both formaldehyde-reduced and sodium-borohydride reduced samples when the Pd loading did not exceed 4 wt%. In case the M/A ratio is higher than 0.5, i.e. Pd loading is higher than 4 wt%, an excess of Pd ions remains in solution. This excess of ions is not expected to be adsorbed on the support and likely undergoes reduction in the solution to form metallic particles. Such unsupported particles are more prone to growth or agglomeration until their precipitation on the support (or on the reactor wall). This was clearly observed for the sodium borohydride-reduced Pd/CNT-Ox samples, where large particle formation occurred upon increasing the nominal Pd loading above 4 wt%. To confirm that large particles are formed by reduction of excess metal precursor, a Pd/CNT-ox sample was prepared with a nominal loading of 15 wt%. The sample was washed before reduction by $NaBH_4$, removing excess metal precursor. Indeed, this sample had Pd particles of 1.0 ± 0.3 nm and very few larger particles (Fig. S10). However, the Pd loading of this sample was only 2.3 wt% (ICP).

The higher concentration of acidic functional groups in AC-ox allowed obtaining higher weight loadings without forming larger particles. Nonfunctionalized CNTs had virtually no acidic functional groups and when used as support ($M/A \gg 0.5$), no adsorption of the metal precursor could occur and therefore only large particles were formed during reduction (Fig. 2a).

3.4. Impact of the reducing agent

Reduction by sodium borohydride led to both small and large particles, while formaldehyde was likely not able to reduce excess metal precursor ions, since only small particles were observed in the formaldehyde-reduced samples supported on functionalized carbons, and loadings above M/A ratios of 0.5 were not obtained. Here we hypothesize that such difference compared to sodium borohydride might stem from the ability of metallic Pd to catalyze the decomposition of formaldehyde [28].

3.5. Amount and formation of large particles

In the XRD patterns, Pd peaks were only observed for the samples that contained large particles. This allowed for a semi-quantitative determination of the amount of Pd in large particles. For this, the XRD patterns were deconvoluted (Figure S9b) and the areas of the Pd (1 1 1) peaks were determined. These areas were normalized against the sum of the areas of the C (1 0 0) and C (1 0 1) peaks. This normalization was performed to correct for effects of parameters such as the amount of sample, the integration time and X-ray absorption within the sample. The peak ratio obtained this way was assumed proportional to the concentration of the sample component (Pd) forming the peak. As only the larger particles were contributing to the peak, the peak ratio was directly proportional to the amount of Pd in the larger particles. An indication of the absolute amount of metal producing the peak was obtained by comparing the obtained peak ratio to the peak ratio of reference catalysts. For this, three reference samples were used consisting of ~4 wt% Pd (crystallite size ~4 nm) supported on the same support (CNT-Ox) prepared by ion adsorption followed by thermal activation at 500 °C in N_2 (details on preparation and structure are described elsewhere [23]). Results of the deconvolution and quantification are shown in Fig. 3 for CNT-Ox supported catalysts. The Pd (1 1 1) peak was not observed at low loadings but appeared at higher loadings and increased linearly above an M/A ratio of 0.5, corresponding to Pd loadings above 4 wt%. The largest peak area for Pd (1 1 1), for sample 10Pd/CNT-Ox_H, corresponded to a Pd loading of 6.3 wt%, while the total Pd loading of this sample was 9.6 wt%. As only the larger (>10 nm according to STEM analysis) Pd particles contribute to the XRD peak, it was concluded that about 65% of the metal had ended up in the larger particles. Similarly, in samples 8Pd/CNT-Ox_H and 4Pd/CNT-Ox_H, 47% and 20% of the metal was located in large particles, respectively. Although the data obtained this way is not fully quantitative, this method provided an estimate of the amount of Pd ending up in large particles.

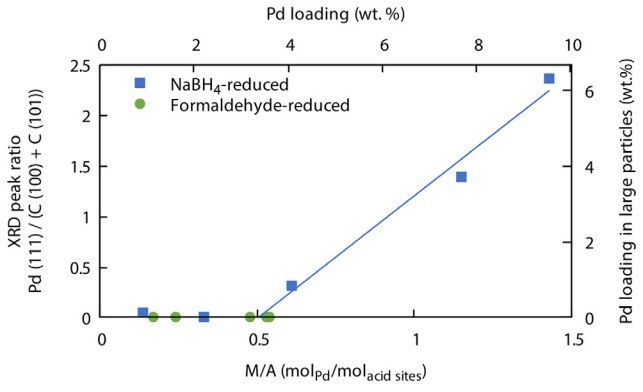

Fig. 3. Peak area of the Pd (1 1 1) diffraction peak normalized against C (1 0 0) and C (1 0 1) for sodium borohydride-reduced and formaldehyde-reduced Pd/CNT-Ox catalysts as a function of the Pd loading (upper x-axis) and M/A ratio with M = amount of Pd (ICP, Table 2) and A = amount of acid sites on the unloaded support (Table 1) (lower x-axis). For an impression on the Pd loading in large particles (right axis), diffraction peak ratios were normalized to reference Pd/CNT-Ox samples with ~4 nm Pd crystallites (more details in supporting information). Large particles are defined as all particles that consist of crystallites observed in XRD, with a particle size >10 nm determined from STEM analysis.

It is important to note that the observations above also suggest that the acid sites with which the metal precursor ions initially interact can only be used once. Should this not be the case, adsorption of a metal precursor ions from the solution could continue considering that during the reduction adsorbed metal precursor ions migrate to form particles and thus free up the support functional groups for further adsorption. To verify the inactivity of acid sites, a potentiometric titration was performed on catalyst sample 4Pd/CNT-Ox_F. No acidic functional groups were detected in this catalyst. This indicates that the acidic functional groups were removed through reaction with the metal precursor [16] or the reducing agent. It is unlikely that the acidic functional groups were fully blocked by coordinated metal atoms as the initially adsorbed metal atoms had clustered to form ~1 nm metal particles (observed in TEM images) containing many atoms and therefore occupying only a small fraction of the surface. Furthermore, the results suggest that at higher Pd loadings interplay between ion adsorption followed by reduction of adsorbed ions and deposition-precipitation of ions reduced in solution took place. This highlights the complexity of the liquid-phase reduction process and different effects the support surface chemistry, the concentration of metal precursor and the type of reducing agent can have on metal particle size and size distribution.

3.6. Catalytic performance

The performance of the catalysts was determined for the catalytic hydrogenation of cinnamaldehyde. This reaction is known as a structure-sensitive reaction: the selectivity towards hydrocinnamaldehyde decreases with increasing particle size [23,29]. Furthermore, an increase of the average metal particle size at constant loading leads to a lower number of metal atoms at the surface, and therefore to a lower activity. All tested samples were active as catalyst for the hydrogenation of cinnamaldehyde (Table 3 and Fig. S12). Full cinnamaldehyde conversion was reached in all cases. The catalytic performance of the catalyst did not decrease over time (cf. Fig. S12), so no clear deactivation was observed. The two formaldehyde-reduced samples had comparable selectivity and Pd-weight normalized activity. Sodium borohydride-reduced samples showed decreasing selectivity towards hydrocinnamaldehyde and Pd-weight normalized activity with increasing Pd loading. No cinnamyl alcohol was formed and no other products were observed in the GC spectra.

The increase in Pd-weight normalized activity and selectivity with decreasing weight loading observed for the sodium borohydride-reduced samples can be explained by the increasing fraction of Pd in small particles (Fig. 4). For the formaldehyde-

Table 3
Catalytic activity and selectivity towards hydrocinnamaldehyde (p = 10 bar H_2, T = 60 °C, t = 200–350 min).

Sample	Activity[a] (mmol g_{Pd}^{-1} s^{-1})	Selectivity[b]
1Pd/CNT-Ox_F	3.2	82%
4Pd/CNT-Ox_F	3.4	82%
1Pd/CNT-Ox_H	3.8	86%
4Pd/CNT-Ox_H	2.4	66%
10Pd/CNT-Ox_H	0.8	47%

[a] Activity at 50% conversion, determined from a linear fit on $\ln(x_{cinnamaldehyde})$ vs. t (see Fig. S12 and supporting information for details on the calculation).
[b] Selectivity at 50% conversion.

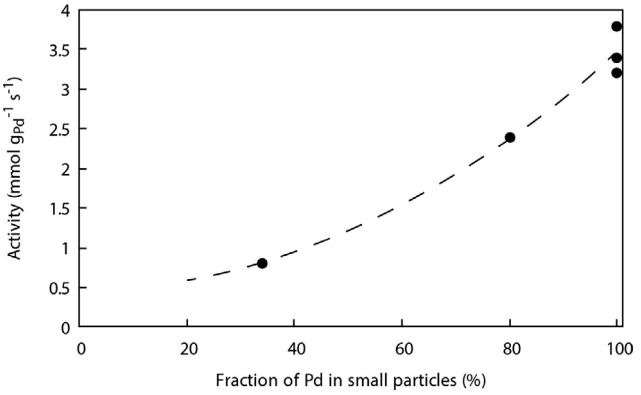

Fig. 4. Catalytic activity plotted against the fraction of Pd in small particles. Fraction of Pd in small particles was calculated as ([weight loading Pd (ICP)]-[Pd loading in large particles (Fig. 3)])/[weight loading Pd (ICP)]. The line has been added to guide the eye.

reduced samples, selectivities and Pd-weight normalized activities were similar, since both catalysts had well dispersed Pd particles and narrow Pd particle size distributions. After catalysis, the ~1 nm Pd particles had increased, to 1.3–2.3 nm (Table S4) with limited impact on results shown in Fig. 4. Due to the limited size increase and the absence of clear deactivation it was expected that the catalysts were reusable. However, the small amount of catalyst used impeded catalyst recycle experiments.

4. Conclusions

This study reports various factors that affect dispersion of Pd/C catalysts prepared by liquid-phase reduction. It was shown that dispersion and size distribution is strongly dependent on the presence of functional groups on the support surface, the type of reducing agent as well as the concentration of metal ions in solution. It was argued that acid functional groups serve as adsorption sites to which Pd precursor ions can bind. After reduction and drying at 120 °C in air, uniformly distributed 1 nm Pd nanoparticles had formed with a narrow particle size distribution, irrespective of the type of reducing agent. However, once the amount of Pd ions surpassed the amount of available acid sites for adsorption, the excess of Pd ions was likely reduced in solution which led to the formation and precipitation of larger (>10 nm) Pd particles when sodium borohydride was used as a reducing agent. Up to 65% of the Pd ended up in the larger particles at the highest loading (10 wt%) on CNT-Ox, this led to a 4-fold decrease in the Pd-weight normalized catalytic activity for the hydrogenation of cinnamaldehyde. Liquid-phase reduction is a complex process and the findings suggest an interplay between ion adsorption and reduction of adsorbed metal ions on the one hand, and precipitation of metal particles that are formed by reduction of metal ions in the solution on the other hand. Precipitation of larger Pd particles could be suppressed by using less metal precursor than the amount of available acid sites, or by choosing formaldehyde as reducing agent that was not able to reduce the metal precursor in solution. The importance of acid sites was confirmed by using nonfunctionalized CNT as support, for which very low loadings of poorly dispersed Pd were achieved. Furthermore, when functionalized activated carbon was used, the higher amount of acid sites allowed for higher Pd loadings to be achieved while maintaining highly dispersed Pd particles. This study proves that preparation of Pd/C catalysts with a high Pd loading and high dispersion via liquid-phase reduction is possible, and the underlying principles reported can be applied to the preparation of other catalytic systems that involve liquid-phase reduction.

Acknowledgements

The authors acknowledge the support of BASF Nederland B.V (BASF Netherlands). K.P.d.J. further acknowledges the European Research Council, EU FP7 ERC Advanced Grant no. 338846. S.H. and N.M. are greatly thankful to Pierre Eloy for collecting and analyzing XPS data.

Appendix A. Supplementary material

Supplementary data to this article can be found online at https://doi.org/10.1016/j.jcat.2019.06.034.

References

[1] J. Zecevic, G. Vanbutsele, K.P. De Jong, J.A. Martens, Nanoscale intimacy in bifunctional catalysts for selective conversion of hydrocarbons, Nature 528 (2015) 245–254, https://doi.org/10.1038/nature16173.
[2] D.W. Lee, B.R. Yoo, Advanced metal oxide (supported) catalysts: synthesis and applications, J. Ind. Eng. Chem. 20 (2014) 3947–3959, https://doi.org/10.1016/j.jiec.2014.08.004.
[3] O. Deutschmann, H. Knözinger, K. Kochloefl, T. Turek, Heterogeneous catalysis and solid catalysts, 2. Development and types of solid catalysts, Ullmann's Encycl, Ind. Chem. (2012) 223–269, https://doi.org/10.1002/14356007.o05.
[4] D. Sanfilippo, P.N. Rylander, Hydrogenation and dehydrogenation, in: Ullmann's Encycl. Ind. Chem., Wiley-VCH Verlag GmbH & Co. KGaA, Weinheim, Germany, 2009, pp. 131–139, https://doi.org/10.1002/14356007.a13_487.pub2.
[5] H.-U. Blaser, A. Indolese, A. Schnyder, H. Steiner, M. Studer, Supported palladium catalysts for fine chemicals synthesis, J. Mol. Catal. A Chem. 173 (2001) 3–18, https://doi.org/10.1016/S1381-1169(01)00143-1.
[6] G. Prieto, J. Zečević, H. Friedrich, K.P. De Jong, P.E. De Jongh, Towards stable catalysts by controlling collective properties of supported metal nanoparticles, Nat. Mater. 12 (2013) 34–39, https://doi.org/10.1038/nmat3471.
[7] R. Ouyang, J.X. Liu, W.X. Li, Atomistic theory of ostwald ripening and disintegration of supported metal particles under reaction conditions, J. Am. Chem. Soc. 135 (2013) 1760–1771, https://doi.org/10.1021/ja3087054.
[8] A. Deffernez, S. Hermans, M. Devillers, Pd/C catalysts prepared by controlled adsorption of Pd(II) species on SX PLUS carbon in the aqueous phase, J. Phys. Chem. C 111 (2007) 9448–9459, https://doi.org/10.1021/jp070402u.
[9] S. Banerjee, K. Dasgupta, A. Kumar, P. Ruz, B. Vishwanadh, J.B. Joshi, V. Sudarsan, Comparative evaluation of hydrogen storage behavior of Pd doped carbon nanotubes prepared by wet impregnation and polyol methods, Int. J. Hydrogen Energy 40 (2015) 3268–3276, https://doi.org/10.1016/j.ijhydene.2015.01.048.
[10] T.K. Das, S. Banerjee, M. Pandey, B. Vishwanadh, R.J. Kshirsagar, V. Sudarsan, Effect of surface functional groups on hydrogen adsorption properties of Pd dispersed reduced graphene oxide, Int. J. Hydrogen Energy 42 (2017) 8032–8041, https://doi.org/10.1016/j.ijhydene.2016.12.024.
[11] B. Wang, T. Yan, T. Chang, J. Wei, Q. Zhou, S. Yang, T. Fang, Palladium supported on reduced graphene oxide as a high- performance catalyst for the dehydrogenation of dodecahydro- N - ethylcarbazole, Carbon 122 (2017) 9–18, https://doi.org/10.1016/j.carbon.2017.06.021.
[12] T. Truong-Huu, K. Chizari, I. Janowska, M.S. Moldovan, O. Ersen, L.D. Nguyen, M.J. Ledoux, C. Pham-Huu, D. Begin, Few-layer graphene supporting palladium nanoparticles with a fully accessible effective surface for liquid-phase hydrogenation reaction, Catal. Today 189 (2012) 77–82, https://doi.org/10.1016/j.cattod.2012.04.005.
[13] V.Z. Radkevich, T.L. Senko, K. Wilson, L.M. Grishenko, A.N. Zaderko, V.Y. Diyuk, The influence of surface functionalization of activated carbon on palladium dispersion and catalytic activity in hydrogen oxidation, Appl. Catal. A Gen. 335 (2008) 241–251, https://doi.org/10.1016/j.apcata.2007.11.029.
[14] I. Hachemi, K. Jeništová, P. Mäki-Arvela, N. Kumar, K. Eränen, J. Hemming, D.Y. Murzin, Comparative study of sulfur-free nickel and palladium catalysts in hydrodeoxygenation of different fatty acid feedstocks for production of biofuels, Catal. Sci. Technol. 6 (2016) 1476–1487, https://doi.org/10.1039/c5cy01294e.
[15] T. Janiak, J. Okal, Effectiveness and stability of commercial Pd/C catalysts in the hydrodechlorination of meta-substituted chlorobenzenes, Appl. Catal. B Environ. 92 (2009) 384–392, https://doi.org/10.1016/j.apcatb.2009.08.018.
[16] P.A. Simonov, A.V. Romanenko, I.P. Prosvirin, E.M. Moroz, A.I. Boronin, A.L. Chuvilin, V.A. Likholobov, On the nature of the interaction of H2PdCl4 with the surface of graphite-like carbon materials, Carbon 35 (1997) 73–82, https://doi.org/10.1016/S0008-6223(96)00129-7.
[17] P. Munnik, P.E. de Jongh, K.P. de Jong, Recent developments in the synthesis of supported catalysts, Chem. Rev. 115 (2015) 6687–6718, https://doi.org/10.1021/cr500486u.

[18] C. Prado-Burguete, A. Linares-Solano, F. Rodríguez-Reinoso, C.S.M. de Lecea, The effect of oxygen surface groups of the support on platinum dispersion in Pt/carbon catalysts, J. Catal. 115 (1989) 98–106, https://doi.org/10.1016/0021-9517(89)90010-9.
[19] S. Hermans, C. Diverchy, O. Demoulin, V. Dubois, E.M. Gaigneaux, M. Devillers, Nanostructured Pd/C catalysts prepared by grafting of model carboxylate complexes onto functionalized carbon, J. Catal. 243 (2006) 239–251, https://doi.org/10.1016/j.jcat.2006.07.019.
[20] R. Banerjee, J.L. Contreras-Mora, S.K. Mcquiston, B. Bolton, B. Alsadat, T. Mehrabadi, J.R. Regalbuto, Electrostatic adsorption of platinum onto carbon nanotubes and nanofibers for nanoparticle synthesis, C 4 (2018) 12, https://doi.org/10.3390/c4010012.
[21] R. Arrigo, S. Wrabetz, M.E. Schuster, D. Wang, A. Villa, D. Rosenthal, F. Girsgdies, G. Weinberg, L. Prati, R. Schlögl, D.S. Su, Tailoring the morphology of Pd nanoparticles on CNTs by nitrogen and oxygen functionalization, Phys. Chem. Chem. Phys. 14 (2012) 10523–10532, https://doi.org/10.1039/C2CP40861A.
[22] M.L. Toebes, J.A. van Dillen, K.P. de Jong, Synthesis of supported palladium catalysts, J. Mol. Catal. A Chem. 173 (2001) 75–98, https://doi.org/10.1016/S1381-1169(01)00146-7.
[23] W.S. Lamme, J. Zečević, K.P. de Jong, Influence of metal deposition and activation method on the structure and performance of carbon nanotube supported palladium catalysts, ChemCatChem 10 (2018) 1552–1555, https://doi.org/10.1002/cctc.201701991.
[24] A. Modak, A. Bhaumik, Surface-exposed Pd nanoparticles supported over nanoporous carbon hollow tubes as an efficient heterogeneous catalyst for the CC bond formation and hydrogenation reactions, J. Mol. Catal. A Chem. 425 (2016) 147–156, https://doi.org/10.1016/j.molcata.2016.09.037.
[25] N. Job, J. Marie, S. Lambert, S. Berthon-Fabry, P. Achard, Carbon xerogels as catalyst supports for PEM fuel cell cathode, Energy Convers. Manage. 49 (2008) 2461–2470, https://doi.org/10.1016/j.enconman.2008.03.025.
[26] T.O. Eschemann, W.S. Lamme, R.L. Manchester, T.E. Parmentier, A. Cognigni, M. Rønning, K.P. de Jong, Effect of support surface treatment on the synthesis, structure, and performance of Co/CNT Fischer-Tropsch catalysts, J. Catal. 328 (2015) 130–138, https://doi.org/10.1016/j.jcat.2014.12.010.
[27] Topas 5 Technical Reference Manual, Bruker AXS GmbH, Karlsruhe, Germany, 2014.
[28] G. Ertl, J. Tornau, The catalytic decomposition of formaldehyde on palladium, Zeitschrift Für Phys. Chemie. 104 (1977) 301–308, https://doi.org/10.1524/zpch.1977.104.4-6.301.
[29] F. Jiang, J. Cai, B. Liu, Y. Xu, X. Liu, Particle size effects in the selective hydrogenation of cinnamaldehyde over supported palladium catalysts, RSC Adv. 6 (2016) 75541–75551, https://doi.org/10.1039/C6RA17000E.